Geophysical Research Letters

Supporting Information for

Space-time inconsistencies in the dynamics of water coverage: tracking walking floods

P. Torre Zaffaroni[1,2,3], J. Houspanossian[3], C.M. Di Bella[1,2], E.G. Jobbágy[3]

[1] Instituto de Investigaciones Fisiológicas y Ecológicas Vinculadas a la Agricultura (IFEVA), Facultad de Agronomía, Universidad de Buenos Aires, CONICET, Buenos Aires, Argentina

[2] Departamento de Métodos Cuantitativos y Sistemas de Información, Facultad de Agronomía, Universidad de Buenos Aires, Argentina

[3] Grupo de Estudios Ambientales — IMASL, Universidad Nacional de San Luis & CONICET, San Luis, Argentina

Contents of this file

Text S1.

Attribution of displacement to natural and induced factors

One way to test the influence of multiple continuous variables that might have interactive and/or non-linear effects is through boosted regression trees, which are based on machine learning algorithms capable of determining features' importance while maintaining adequate interpretability (Elith et al., 2008; Radinger et al., 2018). Based on the effect of topography on potential energy guiding the stagnancy of surface water, and of climate regimes in terms of spatial variability of rainfall events, we hypothesized that (1) displacement is fostered by low water convergence, which could be the result of largely flat topographies, highly meandering rivers, increasing aridity. Based on the different allocation of flooding for crops, decoupled from how flooding spreads over a floodplain, and the long-term effect of dam emplacement on the local flooding regime of the altered water course, we further hypothesize that (2) inundation displacement is enhanced by intensely irrigated regions destined to rice production and countered by well-defined lakes, including natural formations and manmade dams and emplacements for storing water.

We selected global datasets related to some of the most relevant aspects in which inundation displacement may be influenced by topography, climate, and large-scale anthropic activity. Figure S1 gathers the geographical distribution of these variables aggregated to each landscape. We obtained information from (1) Global Multi-resolution Terrain Elevation Data (GMTED2010, USGS) to derive three topographical variables: (a) terrain ruggedness (Riley et al., 1999), and slope integrated at (b) local (250m) and (c) regional (5km) levels (Figure S1 a-b); (2) Global database of river width, slope, catchment area, meander wavelength, sinuosity, and discharge (Frasson et al., 2019, and based upon Global River Width from Landsat, Allen & Pavelsky 2018) to derive the average meander wavelength across all riverine segments (between 60°N and 56°S) contained in each landscape (Figure S1c); (3) Global Lake and Wetlands Dataset (GLWD; Lehner & Doll 2004) to derive four hydrological variables: lake, river, floodplain and reservoir coverage fractions per landscape (Figure S1 d-g); (4) TerraClimate (Abatzoglou et al., 2018) to derive the climatological aridity index as the long-term of annual precipitation-to-potential evapotranspiration ratio (Figure S1h); (5) 2015 Anthromes 12K (Ellis et al., 2019) from which we derived three agricultural variables related with water management: rice, irrigated and rainfed coverage fractions per landscape (Figure S1 i-k). We also included the fraction covered by remote woodlands and flooded forests (Figure S1 l-m) as a proxy of one key passive satellite data caveat which can interfere with the depiction of surface water observation by remote sensors onboard satellite platforms.

Text S2.

Sensitivity analysis of the displacement indices to changes in window size

To test the scale-dependency of the displacement phenomena and the two indices we propose to detect and evaluate them, we performed a sensitivity analysis of the distribution and ranking of dext and dtot across different window sizes, downscaling (0.5°x0.5°) and upscaling (3°x3°) from the original, 1°x1° grid. The sensitivity analysis revealed that changes in the scale of the analysis had little effect on the ranking of displacements (both dext and dtot) across different study windows (Figure S3). This suggests that the geographic patterns we observed in our study are relatively robust and are not significantly influenced by the choice of window size. As an example, the ranking of lower to higher performance of the indices across nine windows presented in Figure 2 remains similar across scales (Figure S3).

It should be noted, however, that increasing the scale of analysis to 3° by 3° windows resulted in a slight increase of extreme displacement values. This effect is likely due to the increasing non-synchronicity of flooding episodes over larger areas. For instance, a paramount case would be to compute the global extreme displacement index, which would highlight the dominant northern hemisphere peak surface water extent and its mismatch from the multiple flooding dynamics occurring elsewhere in the world at other times. On the other hand, the dtot index could be enhanced when using smaller analysis windows. This observation may be linked to the greater influence of pixel-level noise from remotely sensed water classification in smaller geographic extents, leading to an increased noise-to-signal ratio.

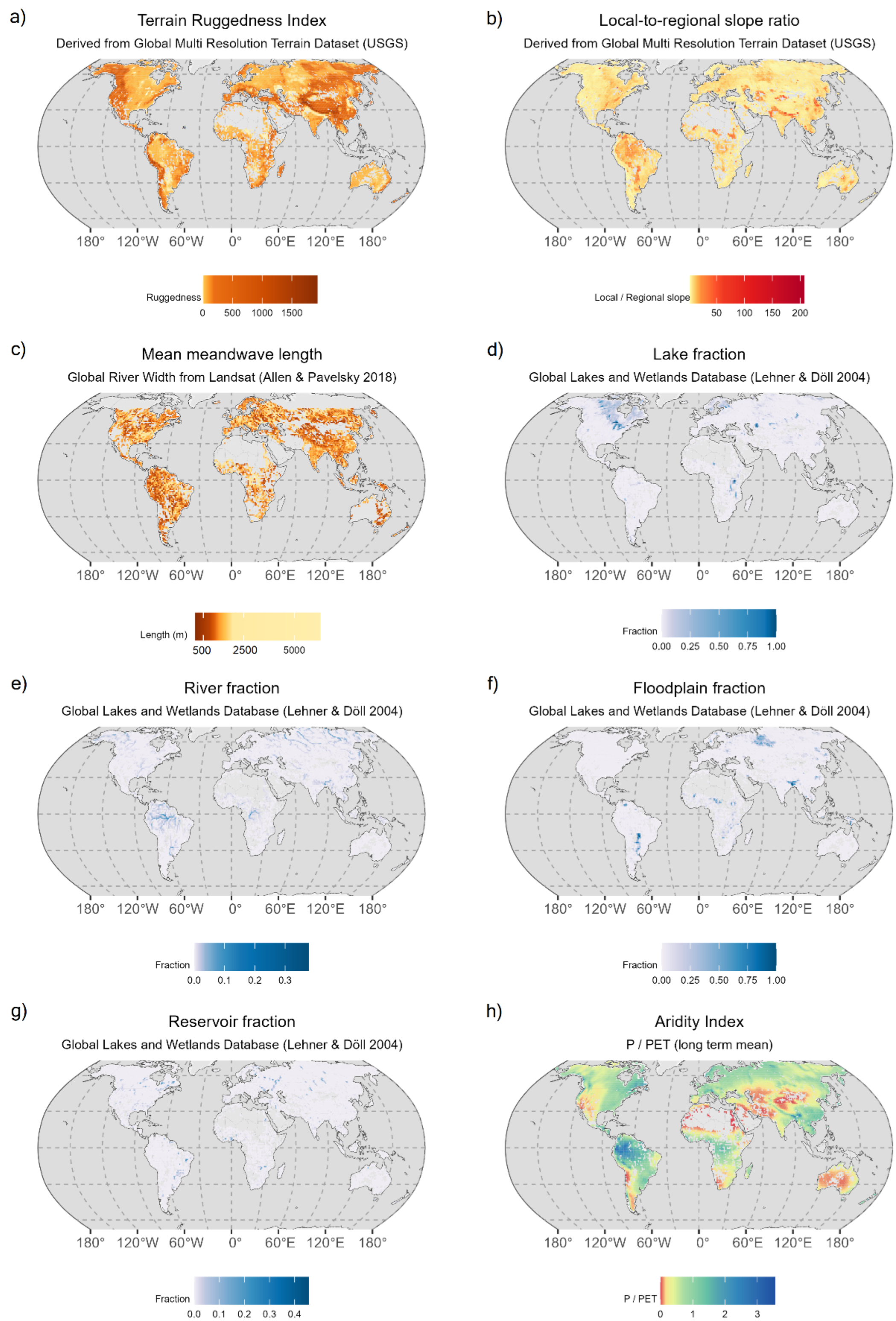

Figure S1. Geographical distribution of the thirteen variables for which we analyzed their influence on inundation displacement: (a) Terrain Ruggedness Index; (b) Local-to-Regional slope ratio; (c) Mean meandwave length; (d) Lake fraction; (e) River fraction; (f) Floodplain fraction; (g) Reservoir fraction; (h) Aridity Index.

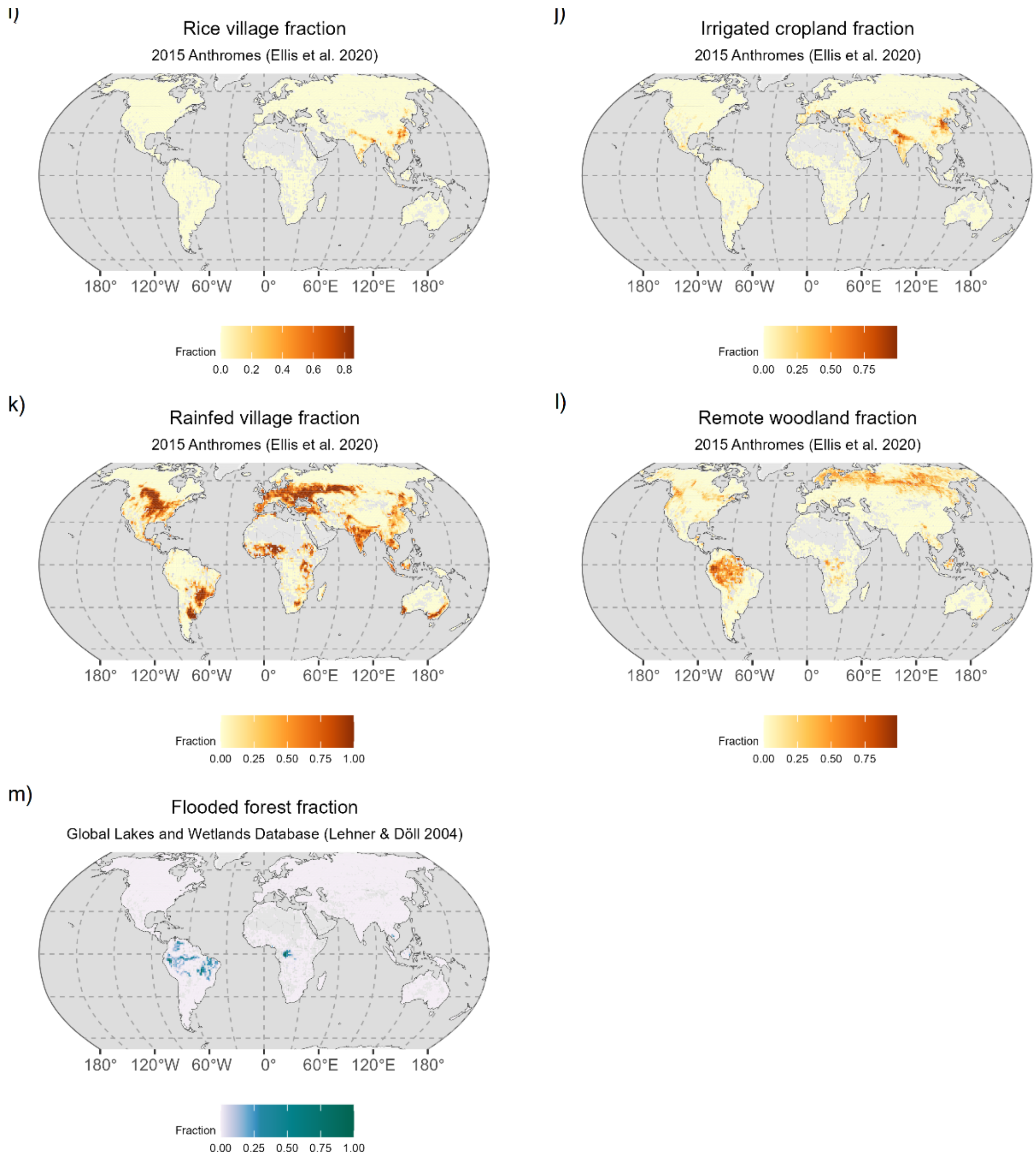

Figure S1 (cont.). Geographical distribution of the thirteen variables for which we analyzed their influence on inundation displacement: (i) Rice fraction; (j) Irrigated cropland fraction; (k) Rainfed fraction; (l) Remote woodland fraction; (m) Flooded forest fraction.

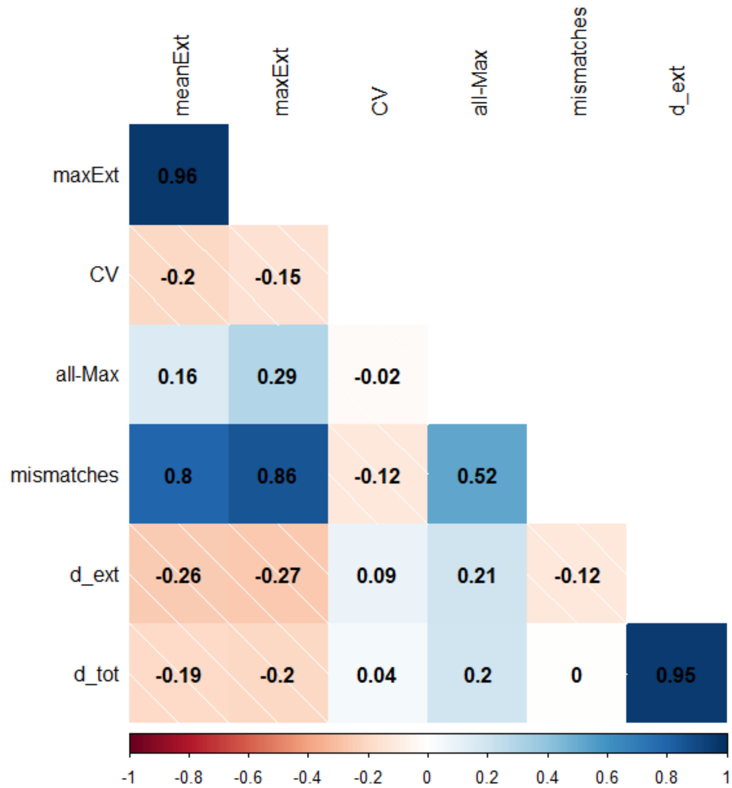

Figure S2. Correlation matrix of typical flooding descriptors and proposed indicators of inundation displacement, all derived from the same dataset (monthly, Landsat-based Global Surface Water; Pekel et al., 2016). Color hue reflects the direction of Spearman's rho correlation (red = negative; blue = positive), while color intensity reflects the strength of the correlation. maxExt = maximum registered flooded extent per 1-degree grid cell at any month between 1985 and 2020; CV = coefficient of variation (mean / sd); all-Max = absolute difference between the sum of all pixels having been flooded at any point between 1985 and 2020, and the maximum registered flooded event (maxExt); mismatches = absolute differences between the null model of coherent flooding development and the actual, pixel-level flooding frequency distribution; d_ext = extreme displacement index (Eq. 1); d_tot = total displacement index (Eq. 2).

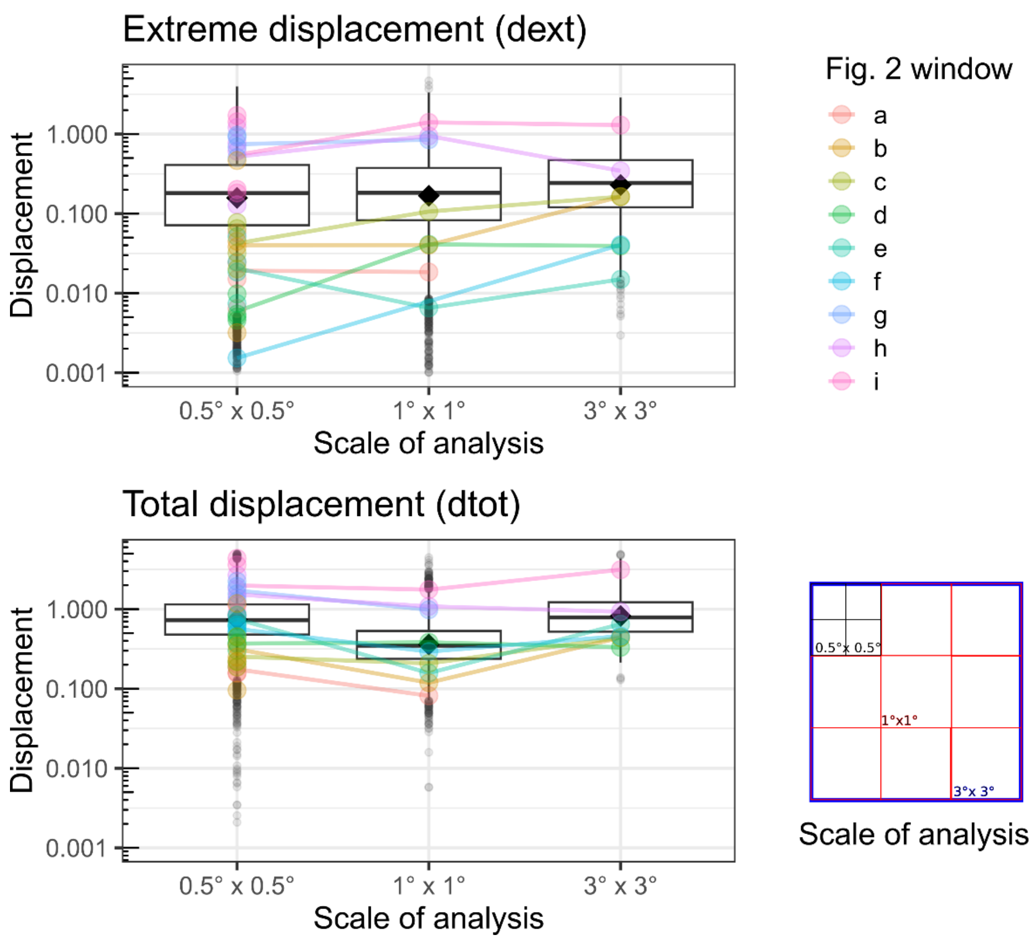

Figure S3. Sensitivity analysis of the two proposed indices (extreme displacement, top; total displacement, bottom) in response to changes in window size by downscaling and upscaling from the original, 1°x1° landscapes. We highlight the performance of each index across the same nine windows depicted in Figure 2.

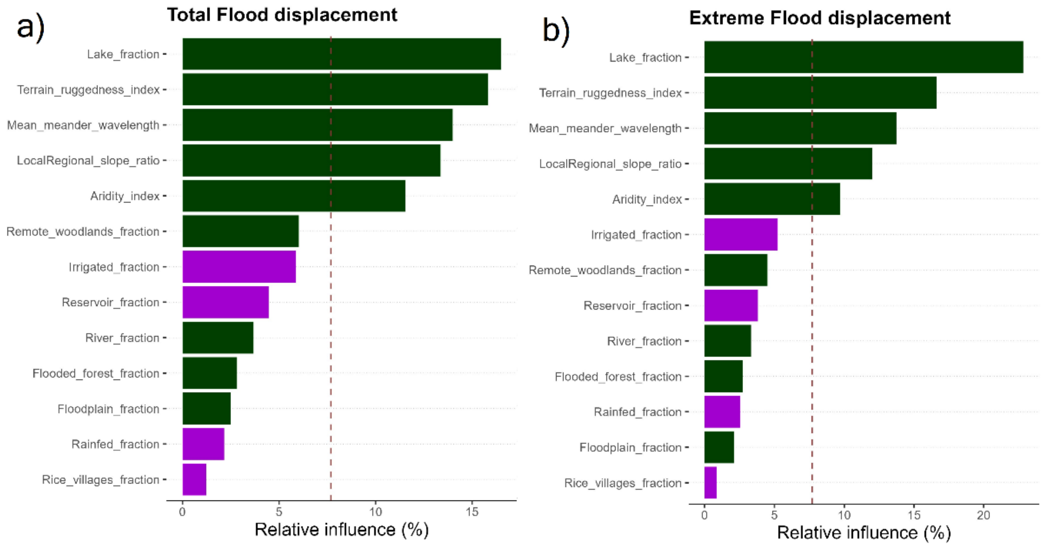

Figure S4. Natural (green) and human (violet) relative influences on (a) total and (b) extreme inundation displacement. Influence values are averaged across a thousand regression tree iterations.

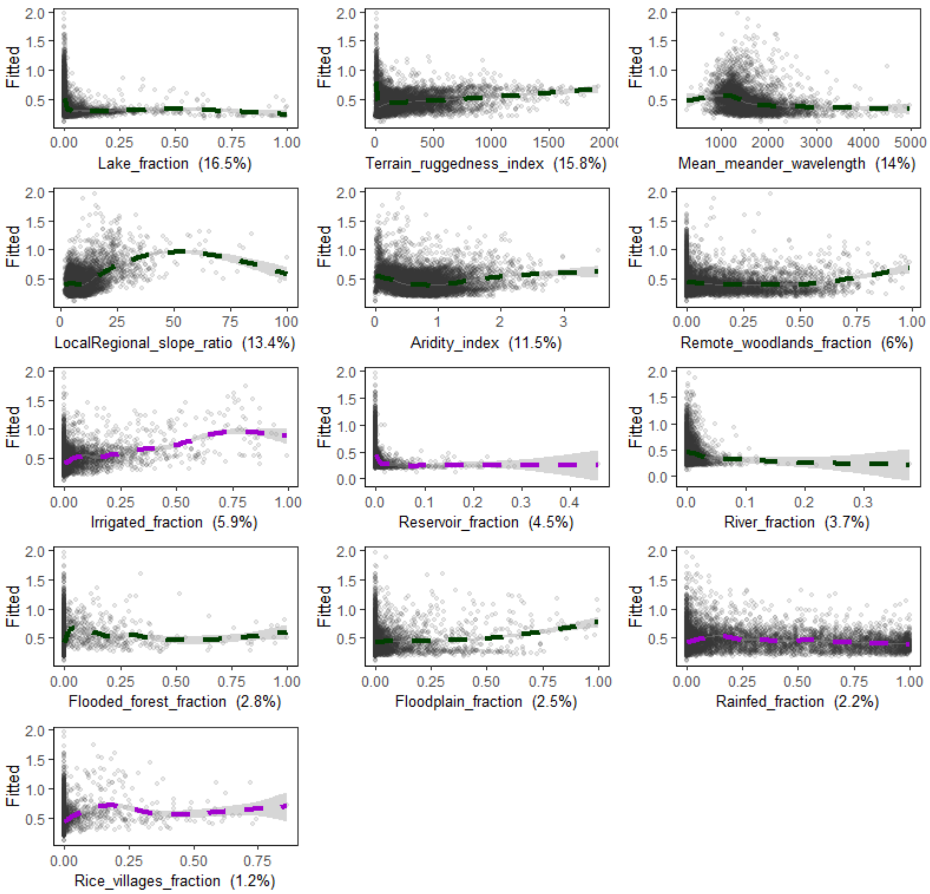

Figure S5. Marginal effect of the natural and induced factors of total inundation displacement (d_{tot}), fitted through general additive models (gam). Values between parenthesis at the x-axis correspond to the relative influence of each variable (averaged across 1000 iterations).

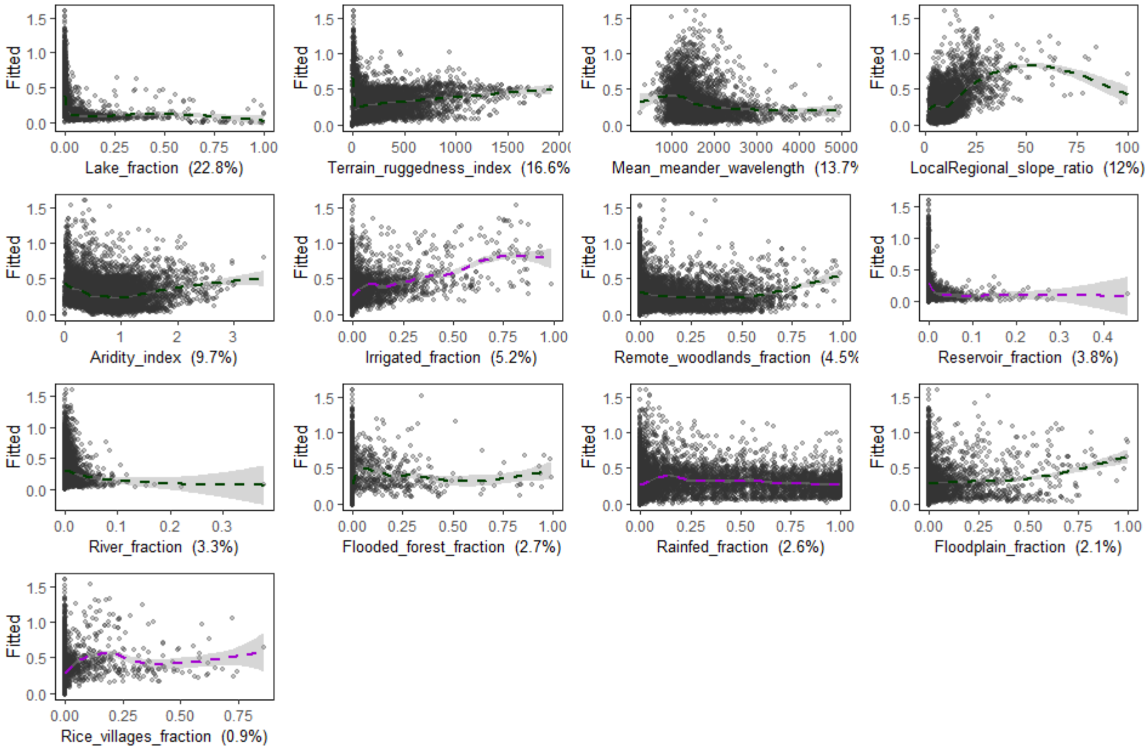

Figure S6. Marginal effect of the natural and induced factors of extreme inundation displacement (d_{ext}), fitted through general additive models (gam). Values between parenthesis at the x-axis correspond to the relative influence of each variable (averaged across 1000 iterations).

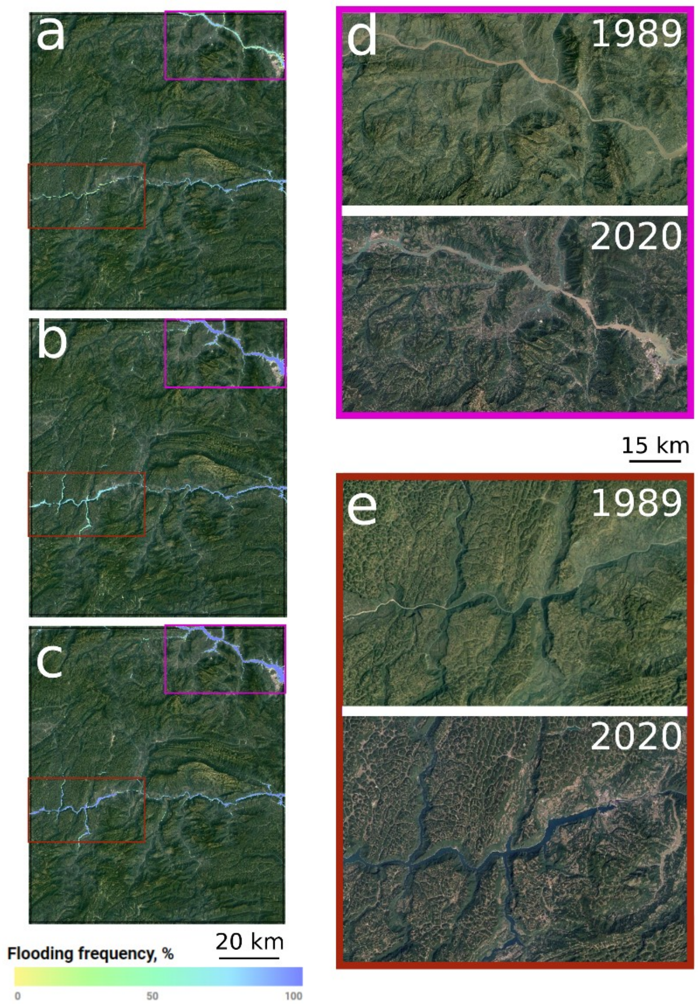

Figure S7. Example of displacement reduction as a result of water reservoir emplacement in a 1°x1° landscape centered at 30.5°N, 110.5°E encompassing the Three Gorges Dam (magenta box) and Shuibuiya Dam (red box) which were built and put into operation between 1994 and 2008. (a-c) geographical distribution of flooding frequency for the periods 1985-2002 (i.e., before the operation of either dam); 2003-2021 (i.e., operational period of the TGD but not SD); and 2009-2021 (i.e., operational period of both dams). (d-e) comparative Google Earth images over the Yangtze River and Qingjiang River, respectively, before and after the emplacement of the dams.

References

Abatzoglou, J. T., Dobrowski, S. Z., Parks, S. A., & Hegewisch, K. C. (2018). *Terraclimate: Monthly climate and climatic water balance for global terrestrial surfaces, university of idaho* [dataset]. Retrieved from https://developers.google.com/earth-engine/datasets/catalog/IDAHO_EPSCOR_TERRACLIMATE doi: 10.1038/sdata.2017.191

Allen, G. H., & Pavelsky, T. (2018). Global extent of rivers and streams. Science, 361 (6402), 585–588. doi: 10.1126/science.aat063

Elith, J., Leathwick, J. R., & Hastie, T. (2008). *A working guide to boosted regression trees* (Vol. 77) (No. 4). John Wiley & Sons, Ltd. doi: 10.1111/j.1365-2656.2008.01390.x

Ellis, E., & Klein Goldewijk, K. (2019). *Anthromes 12k full dataset* [dataset]. Retrieved from https://dataverse.harvard.edu/dataset.xhtml?persistentId=doi:10.7910/DVN/G0QDNQ doi: 10.7910/DVN/G0QDNQ

Frasson, R. P. d. M., Pavelsky, T. M., Fonstad, M. A., Durand, M. T., Allen, G. H., Schumann, G., . . . Yang, X. (2019). *Global database of river width, slope, catchment area, meander wavelength, sinuosity, and discharge* [dataset]. Zenodo. Retrieved from https://doi.org/10.5281/zenodo.2582500 doi: 10.5281/zenodo.2582500

Lehner, B., & D¨oll, P. (2004). *Global lakes and wetlands database: Lakes and wetlands grid (level 3)* [dataset]. World Wildlife Fund. Retrieved from https://www.worldwildlife.org/publications/global-lakes-and-wetlands-database-lakes-and-wetlands-grid-level-3

Pekel, J.-F., Cottam, A., Gorelick, N., & Belward, A. S. (2016a). High-resolution mapping of global surface water and its long-term changes. Nature, 540 (7633), 418–422. doi: 10.1038/nature2058

Radinger, J., Alcaraz-Hernández, J. D., & García-Berthou, E. (2018). *Environmental and spatial correlates of hydrologic alteration in a large Mediterranean river catchment*. Science of The Total Environment, 639, 1138–1147. doi: 10.1016/J.SCITOTENV.2018.05.227

Riley, S., DeGloria, S., & Elliot, R. (1999). *A terrain ruggedness that quantifies topographic heterogeneity*. Intermountain Journal of Science, 5 (1-4), 23–27